ISSN 1070-3284, Russian Journal of Coordination Chemistry, 2020, Vol. 46, No. 9, pp. 639–652. © Pleiades Publishing, Ltd., 2020.
Russian Text © The Author(s), 2020, published in Koordinatsionnaya Khimiya, 2020, Vol. 46, No. 9, pp. 562–576.

Chemisorptive Synthesis, Self-Assembly of Complicated 2D and 3D Supramolecular Architectures (Role of Hydrogen Bonds and Secondary Interactions Au···S and S···Cl), and Thermal Behavior of Pseudo-Polymeric Gold(III)–Mercury(II) Dibutyldithiocarbamato-Chlorido Complexes

A. V. Ivanov[a], *, O. V. Loseva[a], and T. A. Rodina[a]

[a] *Institute of Geology and Nature Management, Far East Branch, Russian Academy of Sciences, Blagoveshchensk, Russia*
**e-mail: alexander.v.ivanov@chemist.com*

Received November 29, 2019; revised December 8, 2019; accepted December 25, 2019

Abstract—The interaction of mercury(II) dibutyl dithiocarbamate (BuDtc) with $[AuCl_4]^-$ anions in 2 M HCl was studied. The heterogeneous reaction of chemisorption binding of gold(III) from the solution leads to heteronuclear Au(III)–Hg(II) pseudo-polymeric complexes of the ionic type: $([Au\{S_2CN(C_4H_9)_2\}_2]_2[Hg_2Cl_6])_n$ (**I**) and $([(C_4H_9)_2NH_2]_{0.5}[Au\{S_2CN(C_4H_9)_2\}_2]_{1.5}[Hg_2Cl_6])_n$ (**II**), whose crystal and supramolecular structures were determined by X-ray diffraction analysis (CIF files CCDC nos. 1965151 (**I**) and 1965152 (**II**)). The cationic part of each compound is represented by two structurally nonequivalent complex ions $[Au\{S_2CN(C_4H_9)_2\}_2]^+$ (A and B) being conformers. The structure of compound **II** additionally contains the dibutylammonium cation. In both cases, binuclear $[Hg_2Cl_6]^{2-}$ is a counterion (centrosymmetric in the structure of compound **I** and noncentrosymmetric in the structure of compound **II**). Owing to the secondary interactions Au···S and S···Cl (as well as hydrogen bonds N–H···Cl in compound **II**), all ionic structural units participate in the construction of pseudo-polymeric cationic and cation-anionic chains, which are combined into a complicatedly organized 2D supramolecular network (in **I**) or 3D framework (in **II**). The thermal behavior of compounds **I** and **II** was studied by simultaneous thermal analysis. The thermolysis of the complexes is accompanied by the quantitative regeneration of bound gold, liberation of $HgCl_2$, and partial transformation of the latter into HgS.

Keywords: mercury(II) dialkyl dithiocarbamates, chemisorption activity, double gold(III)–mercury(II) complexes, supramolecular self-assembly, secondary bonds Au···S and S···Cl, ^{13}C CP-MAS NMR, thermal behavior

DOI: 10.1134/S107032842009002X

INTRODUCTION

The coordination compounds of mercury(II) with chelate ligands are interesting as a basis for photoluminescent and electroluminescent materials [1, 2] and also find use in medicine and agriculture owing to their fungicidal and antibacterial activity [3]. Mercury(II) dithiocarbamates are promising precursors for the production of film and nanosized mercury sulfides with luminescence and semiconductor properties, which are widely used in manufacturing ultrasonic and photoelectrical converters, image sensors, and infrared detectors [4–6].

Dithiocarbamate ligands exhibiting diverse structural functions (monodentate, bidentate-terminal, bidentate-bridging, and tridentate-bridging) and mercury(II) cations (electronic configuration d^{10}) form complexes characterized by complicated supramolecular structures. Relatively weak interactions of the nonvalent type (hydrogen bonds C–H···S; secondary Hg···N, Hg···S, and S···S interactions; π···π and metallophilic interactions) stabilize these supramolecular architectures and also provide the manifestation of the photoluminescence properties of the complexes [7].

We have previously found that freshly precipitated mercury(II) dithiocarbamates are capable of chemisorption binding gold(III) from acidic solutions to form heterometallic gold(III)–mercury(II) dithiocarbamato-chlorido complexes of the ionic type containing various polychloro(di)mercurate(II) ions: $[Au(S_2CNR_2)_2]_2[HgCl_4]$ ($R = CH_3$ [8], $R_2 = (CH_2)_6$ [9]), $[Au(S_2CNR_2)_2]_2[Hg_2Cl_6]$ ($R = C_2H_5$ [8], *iso*-C_3H_7 [10], $R_2 = (CH_2)_5$ [11], $(CH_2)_4O$ [9]), and

$[Au\{S_2CN(CH_2)_6\}_2][HgCl_3]$ [9]. In addition, it is shown that the specific character of the complexes based on the dibutyldithiocarbamate ligands (BuDtc) is determined by the possibility of forming ternary compounds with the general composition $([(C_4H_9)_2NH_2][Au\{S_2CN(C_4H_9)_2\}_2][MCl_4])_n$ (M = Cd [12], Zn [13]). It should be mentioned that all compounds presented above are characterized by complicatedly organized supramolecular structures.

Continuing these studies, in the present work we preparatively isolated two new ion-polymeric gold(III)–mercury(II) complexes as individual forms of binding Au(III) from solutions with freshly precipitated mercury(II) dibutyl dithiocarbamate: $([Au\{S_2CN(C_4H_9)_2\}_2]_2[Hg_2Cl_6])_n$ (**I**) and $([(C_4H_9)_2NH_2]_{0.5}[Au\{S_2CN(C_4H_9)_2\}_2]_{1.5}[Hg_2Cl_6])_n$ (**II**). The synthesized complexes were structurally characterized. The crystal and supramolecular structures, spectral characteristics, and thermal behavior of the complexes were studied by X-ray diffraction analysis (XRD), ^{13}C CP-MAS NMR spectroscopy, and simultaneous thermal analysis (STA).

EXPERIMENTAL

Sodium dibutyl dithiocarbamate was synthesized by the reaction of carbon disulfide (Merck) with dibutylamine (Aldrich) in an alkaline medium, and the initial mercury(II) dibutyl dithiocarbamate was prepared by the precipitation of Hg^{2+} ions from the aqueous phase with a solution of $Na\{S_2CN(C_4H_9)_2\} \cdot H_2O$ taken in a stoichiometric ratio [14]. According to the XRD data, $[Hg_2\{S_2CN(C_4H_9)_2\}_4]$ is a binuclear complex, whose structural feature is the stabilization of the central tricyclic fragment $[Hg_2S_4C_2]$ in the bath conformation [15].

Synthesis of complexes I and II. A solution of $AuCl_3$ (10 mL, in 2 M HCl) containing gold in an amount of 32.0 mg was poured to $[Hg_2\{S_2CN(C_4H_9)_2\}_4]$ (100 mg), and the mixture was stirred for 30 min. The formed red-brown uniform plastic mixture was separated, washed with water (using simultaneous thorough trituration with a glass stick), dried on the filter, and dissolved in a toluene–acetone (1 : 1) mixture. Yellow crystals of complex **I** (prismatic) and **II** (thin elongated) for XRD experiments were prepared by the slow evaporation of the solvent at room temperature. The crystals were sampled under a microscope. The residual content of gold in the solution was determined on an iCE 3000 atomic absorption spectrometer (Thermo Electron Corporation, USA). The degree of binding gold from the solution was 73.14%.

The heterogeneous reaction of binding gold(III) from the solution with freshly precipitated mercury(II) dibutyl dithiocarbamate affords two heteronuclear ionic gold(III)–mercury(II) complexes and is accompanied by the full redistribution of the ligands between the coordination spheres of Hg(II) and Au(III) with the partial decomposition of the BuDtc ligand

$$3[Hg_2\{S_2CN(C_4H_9)_2\}_4] + 5H[AuCl_4] = [Au\{S_2CN(C_4H_9)_2\}_2]_2[Hg_2Cl_6] + 2[(C_4H_9)_2NH_2]_{0.5}[Au\{S_2CN(C_4H_9)_2\}_2]_{1.5}[Hg_2Cl_6] + 2CS_2 + (C_4H_9)_2NH + 2HCl.$$

The amount of gold(III) bound from the solution to the solid phase (23.4 mg) corresponded to the 86.9% yield of the reaction product.

The crystalline reaction products were characterized by the data of ^{13}C MAS NMR spectroscopy (δ, ppm): 196.0, 195.7, 195.4, 195.1 (1 : 2 : 1 : 1, $>NCS_2^-$); 54.2, 51.5, 51.0 ($>N-{}^{\alpha}CH_2-$); 31.1, 30.6 ($-{}^{\beta}CH_2-$); 21.2, 20.8 ($-{}^{\gamma}CH_2-$); 15.6, 15.2, 14.2 ($-CH_3$).

X-ray diffraction analyses of the single crystals of complexes **I** and **II** were carried out on a Bruker-Nonius X8 Apex CCD diffractometer (MoK_α radiation, λ = 0.71073 Å, graphite monochromator) at 150(2) K. Data were collected using the standard procedure of scanning narrow frames in the φ and ω scan modes. An absorption correction was applied empirically using the SADABS program [16]. The structure was determined by a direct method and refined by least squares (for F^2) in the full-matrix anisotropic approximation of non-hydrogen atoms. The positions of the hydrogen atoms were calculated geometrically and included into the refinement in the riding model. The calculations on structure determination and refinement were performed using the SHELXTL program package [16].

The coordinates of atoms, bond lengths, and angles were deposited with the Cambridge Crystallographic Data Centre (CIF files CCDC nos. 1965151 (**I**) and 1965152 (**II**); deposit@ccdc.cam.ac.uk or http://www.ccdc.cam.ac.uk). The main crystallographic data and results of refinement for the structures of complexes **I** and **II** are presented in Table 1. Selected bond lengths and angles are listed in Table 2. The geometric parameters of the hydrogen bonds of complex **II** are presented in Table 3.

^{13}C CP-MAS NMR spectra were recorded on a Bruker Ascend Aeon spectrometer operating at a frequency of 100.64 MHz in the pulsed Fourier transform mode and having a superconducting magnet (B_0 = 9.4 T) with the closed condensation cycle of helium through an external compressor. Proton cross polarization (CP) was used (contact time $^1H-^{13}C$ 2.0 ms). The suppression of $^{13}C-^1H$ interactions was based on the decoupling effect using a radiofrequency field at the resonance frequency of protons (400.21 MHz) [17]. The crystalline sample (62 mg) was placed in a 4.0-mm ZrO_2 ceramic rotor. When measuring ^{13}C magic-angle-spinning (MAS) NMR spectra, the spinning frequency of the sample at 3200(1) Hz was used. 3200(1) Hz was used (6900 tran-

Table 1. Crystallographic data, experimental characteristics, and structure refinement parameters for compounds **I** and **II**

Parameter	Value	
	I	**II**
Empirical formula	$C_{36}H_{72}N_4S_8Cl_6Au_2Hg_2$	$C_{31}H_{64}N_{3.5}S_6Cl_6Au_{1.5}Hg_2$
FW	1825.27	1587.55
Crystal system	Triclinic	Monoclinic
Space group	$P\bar{1}$	$P2_1/c$
a, Å	10.6399(3)	11.7618(8)
b, Å	11.6712(3)	25.0159(18)
c, Å	12.7780(3)	17.5347(13)
α, deg	103.3450(10)	90.00
β, deg	101.5940(10)	105.387(2)
γ, deg	107.4260(10)	90.00
V, Å^3	1409.34(6)	4974.3(6)
Z	1	4
ρ_{calc}, g/cm^3	2.151	2.120
μ, mm^{-1}	11.229	11.167
F(000)	864	3004
Crystal size, mm	0.24 × 0.20 × 0.13	0.28 × 0.08 × 0.08
Range of data collection over θ, deg	1.71–27.59	1.63–27.65
Ranges of reflection indices	$-13 \le h \le 13$, $-15 \le k \le 15$, $-15 \le l \le 16$	$-14 \le h \le 15$, $-32 \le k \le 32$, $-22 \le l \le 22$
Measured reflections	14479	48505
Independent reflections (R_{int})	6499 (0.0264)	11481 (0.0308)
Reflections with $I > 2\sigma(I)$	5749	9642
Refinement variables	269	501
GOOF	0.992	1.028
R factors for $F^2 > 2\sigma(F^2)$	$R_1 = 0.0240$, $wR_2 = 0.0441$	$R_1 = 0.0236$, $wR_2 = 0.0419$
R factors for all reflections	$R_1 = 0.0297$, $wR_2 = 0.0455$	$R_1 = 0.0348$, $wR_2 = 0.0437$
Residual electron density (min/max), e/Å^3	−0.931/0.984	−0.972/1.054

sients, spaced by relaxation delays of 2.0 s, were accumulated; duration of proton π/2 pulses 2.7 μs). Isotropic ^{13}C chemical shifts (ppm) were given relatively to one of the signals of solid adamantane (at δ = 38.48 ppm relative to tetramethylsilane) that was used as an external standard with a correction to the drift of the magnetic field, whose frequency equivalent was 0.025 Hz/h.

Thermal behavior of complexes I and **II** was studied by the STA method on an STA 449C Jupiter instrument (NETZSCH) in corundum crucibles under caps with a hole providing a vapor pressure of 1 atm upon the thermal decomposition of the sample. The heating rate was 5°C/min to 1100°C in an argon atmosphere. The weight of the samples was 2.011–5.448 mg. The accuracy of temperature measurement was ±0.7°C, and the accuracy of weight change was $\pm 1 \times 10^{-4}$ mg. The correction file and temperature and sensitivity calibrations at a specified temperature program and heating rate were used when recording the thermogravimetry (TG) and differential scanning calorimetry (DSC) curves. The independent determination of melting points was performed on a PTP(M) instrument (OAO Khimlaborpribor).

RESULTS AND DISCUSSION

The crystal structures of the complexes were solved by the XRD method in order to determine their structural organization and supramolecular self-organiza-

Table 2. Selected bond lengths (*d*) and bond (ω) and torsion (φ) angles in the structures of compounds **I** and **II***

I

Bond	*d*, Å	Bond	*d*, Å
Au(1)–S(1)	2.3318(9)	Au(2)···S(1)[a]	3.6608(10)
Au(1)–S(2)	2.3349(9)	S(3)–C(10)	1.741(3)
S(1)–C(1)	1.733(4)	S(4)–C(10)	1.737(3)
S(2)–C(1)	1.739(4)	N(2)–C(10)	1.303(4)
N(1)–C(1)	1.304(4)	N(2)–C(11)	1.482(4)
N(1)–C(2)	1.479(4)	N(2)–C(15)	1.489(4)
N(1)–C(6)	1.479(4)	Hg(1)–Cl(1)	2.6982(9)
Au(2)–S(3)	2.3444(8)	Hg(1)–Cl(2)	2.3662(10)
Au(2)–S(4)	2.3328(8)	Hg(1)–Cl(3)	2.3984(9)
		Hg(1)–Cl(1)[c]	2.5653(10)
Angle	ω, deg	Angle	ω, deg
S(1)Au(1)S(2)	75.72(3)	Au(2)S(4)C(10)	86.89(11)
S(1)Au(1)S(2)[a]	104.28(3)	S(3)C(10)S(4)	111.06(17)
Au(1)S(1)C(1)	86.62(11)	Cl(1)Hg(1)Cl(2)	107.71(4)
Au(1)S(2)C(1)	86.39(12)	Cl(1)Hg(1)Cl(3)	101.02(3)
S(1)C(1)S(2)	111.20(17)	Cl(1)Hg(1)Cl(1)[c]	89.47(3)
S(3)Au(2)S(4)	75.62(3)	Cl(2)Hg(1)Cl(3)	127.46(4)
S(3)Au(2)S(4)[b]	104.38(3)	Cl(2)Hg(1)Cl(1)[c]	115.42(4)
Au(2)S(3)C(10)	86.43(10)	Cl(3)Hg(1)Cl(1)[c]	107.72(3)
		Hg(1)Cl(1)Hg(1)[c]	90.53(3)
Angle	φ, deg	Angle	φ, deg
Au(1)S(1)S(2)C(1)	176.9(2)	Au(2)S(3)S(4)C(10)	–179.7(2)
S(1)Au(1)C(1)S(2)	177.2(2)	S(3)Au(2)C(10)S(4)	–179.7(2)
S(1)C(1)N(1)C(2)	0.7(5)	S(3)C(10)N(2)C(11)	–4.0(5)
S(1)C(1)N(1)C(6)	–177.0(3)	S(3)C(10)N(2)C(15)	180.0(3)
S(2)C(1)N(1)C(2)	–179.4(3)	S(4)C(10)N(2)C(11)	174.5(3)
S(2)C(1)N(1)C(6)	2.9(5)	S(4)C(10)N(2)C(15)	–1.5(5)

II

Bond	*d*, Å	Bond	*d*, Å
Au(1)–S(1)	2.3274(9)	S(6)–C(19)	1.737(3)
Au(1)–S(2)	2.3323(10)	N(2)–C(10)	1.306(4)
Au(1)···S(6)	3.5698(9)	N(2)–C(11)	1.476(4)
S(1)–C(1)	1.727(4)	N(2)–C(15)	1.473(4)
S(2)–C(1)	1.737(4)	N(3)–C(19)	1.300(4)
N(1)–C(1)	1.306(4)	N(3)–C(20)	1.490(4)
N(1)–C(2)	1.479(5)	N(3)–C(24)	1.487(4)
N(1)–C(6)	1.471(5)	N(4)–C(28)	1.377(16)
Au(2)–S(3)	2.3478(9)	N(4)–C(32)	1.459(13)
Au(2)–S(4)	2.3415(9)	Hg(1)–Cl(1)	2.3660(10)
Au(2)–S(5)	2.3398(9)	Hg(1)–Cl(2)	2.3668(10)
Au(2)–S(6)	2.3326(9)	Hg(1)–Cl(3)	2.6963(9)

Table 2. (Contd.)

II			
Bond	*d*, Å	Bond	*d*, Å
Au(2)···S(1)	3.2948(9)	Hg(1)–Cl(4)	2.6200(9)
Au(2)···S(5)[b]	3.8655(9)	Hg(2)–Cl(3)	2.6564(9)
S(3)–C(10)	1.741(3)	Hg(2)–Cl(4)	2.6360(9)
S(4)–C(10)	1.725(3)	Hg(2)–Cl(5)	2.3661(10)
S(5)–C(19)	1.736(3)	Hg(2)–Cl(6)	2.3879(10)
Angle	ω, deg	Angle	ω, deg
S(1)Au(1)S(2)	75.30(3)	S(5)C(19)S(6)	110.7(2)
S(1)Au(1)S(2)[a]	104.70(3)	Cl(1)Hg(1)Cl(2)	132.78(4)
Au(1)S(1)C(1)	87.26(13)	Cl(1)Hg(1)Cl(3)	104.42(4)
Au(1)S(2)C(1)	86.87(12)	Cl(1)Hg(1)Cl(4)	114.39(4)
S(1)C(1)S(2)	110.5(2)	Cl(2)Hg(1)Cl(3)	101.79(3)
S(3)Au(2)S(4)	75.27(3)	Cl(2)Hg(1)Cl(4)	105.38(4)
S(3)Au(2)S(5)	105.61(3)	Cl(3)Hg(1)Cl(4)	87.26(3)
S(3)Au(2)S(6)	178.95(3)	Cl(3)Hg(2)Cl(4)	87.76(3)
S(4)Au(2)S(5)	178.58(3)	Cl(3)Hg(2)Cl(5)	106.31(3)
S(4)Au(2)S(6)	103.75(3)	Cl(3)Hg(2)Cl(6)	106.23(4)
S(5)Au(2)S(6)	75.37(3)	Cl(4)Hg(2)Cl(5)	108.92(4)
Au(2)S(3)C(10)	86.36(12)	Cl(4)Hg(2)Cl(6)	104.35(4)
Au(2)S(4)C(10)	86.92(12)	Cl(5)Hg(2)Cl(6)	133.72(4)
Au(2)S(5)C(19)	86.86(12)	Hg(1)Cl(3)Hg(2)	89.92(3)
Au(2)S(6)C(19)	87.06(12)	Hg(1)Cl(4)Hg(2)	92.05(3)
S(3)C(10)S(4)	111.4(2)		
Angle	φ, deg	Angle	φ, deg
Au(1)S(1)S(2)C(1)	177.9(2)	S(5)Au(2)C(19)S(6)	178.6(2)
S(1)Au(1)C(1)S(2)	178.1(2)	S(3)C(10)N(2)C(11)	–0.8(5)
S(1)C(1)N(1)C(2)	–4.4(5)	S(3)C(10)N(2)C(15)	175.9(2)
S(1)C(1)N(1)C(6)	175.8(3)	S(4)C(10)N(2)C(11)	–178.3(2)
S(2)C(1)N(1)C(2)	174.8(3)	S(4)C(10)N(2)C(15)	–1.6(5)
S(2)C(1)N(1)C(6)	–5.0(5)	S(5)C(19)N(3)C(20)	1.6(5)
Au(2)S(3)S(4)C(10)	179.6(2)	S(5)C(19)N(3)C(24)	–178.6(2)
Au(2)S(5)S(6)C(19)	178.4(2)	S(6)C(19)N(3)C(20)	–179.1(2)
S(3)Au(2)C(10)S(4)	179.6(2)	S(6)C(19)N(3)C(24)	0.6(5)

* Symmetry transforms: [a] $-x, -y, 1-z$; [b] $1-x, -y, 1-z$; [c] $1-x, 1-y, -z$ (**I**); [a] $-x, 1-y, 1-z$; [b] $1-x, 1-y, 1-z$ (**II**).

tion. The unit cells of complexes **I**/**II** include 1/4 formula units $[Au\{S_2CN(C_4H_9)_2\}_2]_2[Hg_2Cl_6]/[(C_4H_9)_2NH_2]_{0.5}[Au\{S_2CN(C_4H_9)_2\}_2]_{1.5}[Hg_2Cl_6]$ (Fig. 1, Table 1). The cationic part of compound **I** contains two structurally nonequivalent centrosymmetric complex cations $[Au\{S_2CN(C_4H_9)_2\}_2]^+$: cation A with the Au(1) atom and cation B with Au(2) (Figs. 2a, 2b). Along with two nonequivalent gold(III) cations: centrosymmetric cation A (Au(1)) and noncentrosymmetric cation B (Au(2)), the structure of compound **II** also includes the dibutylammonium cation (Figs. 3a–3c, Table 2).

The BuDtc ligands are characterized by two common features: the mutual arrangement of atoms in the S_2CNC_2 groups is close to coplanar (see the corresponding torsion angles in Table 2), and the N–C(S)S bonds are substantially shorter (1.300–1.306 Å) than the N–CH_2 bonds (1.471–1.490 Å). The C–C bond lengths range from 1.464(17) to 1.514(9) Å. Both facts are a direct consequence of the manifestation of the

Table 3. Geometric parameters of hydrogen bonds in complex **II***

Contact N–H···Cl	Distance, Å			Angle N–H···Cl, deg
	N–H	H···Cl	N···Cl	
N(4)–H(41)···Cl(3)	0.92	2.53	3.412(7)	160.2
N(4)–H(42)···Cl(6)[d]	0.92	2.66	3.481(8)	149.2

* Symmetry transform: [d] $1 - x$, $1 - y$, $-z$.

mesomeric effect in the ligands discussed. In each of cations A and B, the central gold atom S,S'-bidentately coordinates two BuDtc ligands forming a homogeneous environment of four sulfur atoms: a square-planar geometry of the [AuS4] polygon indicates a low-spin intraorbital dsp^2 hybrid state of the gold atom. The ligands exhibit an almost isobidentate character of coordination: Au–S is 2.3318–2.3444 Å (**I**) and 2.3274–2.3478 Å (**II**) (Table 2), which results in the formation of two four-membered metallocycles $[AuS_2C]$ linked by the common gold atom. These small-sized cycles exhibit the Au···C (2.822–2.836 Å) and S···S (2.846–2.867 Å) distances, whose values are much less than the sums of the van der Waals radii of the corresponding pairs of atoms (3.36 and 3.60 Å [18, 19]), and their planar geometry is illustrated by the AuSSC and SAuCS torsion angles, which do not differ strongly (by 0.3°–3.1°) from 180° or 0° (Table 2). In spite of the deep structural similarity of the nonequivalent cations $[Au\{S_2CN(C_4H_9)_2\}_2]^+$ in the synthesized

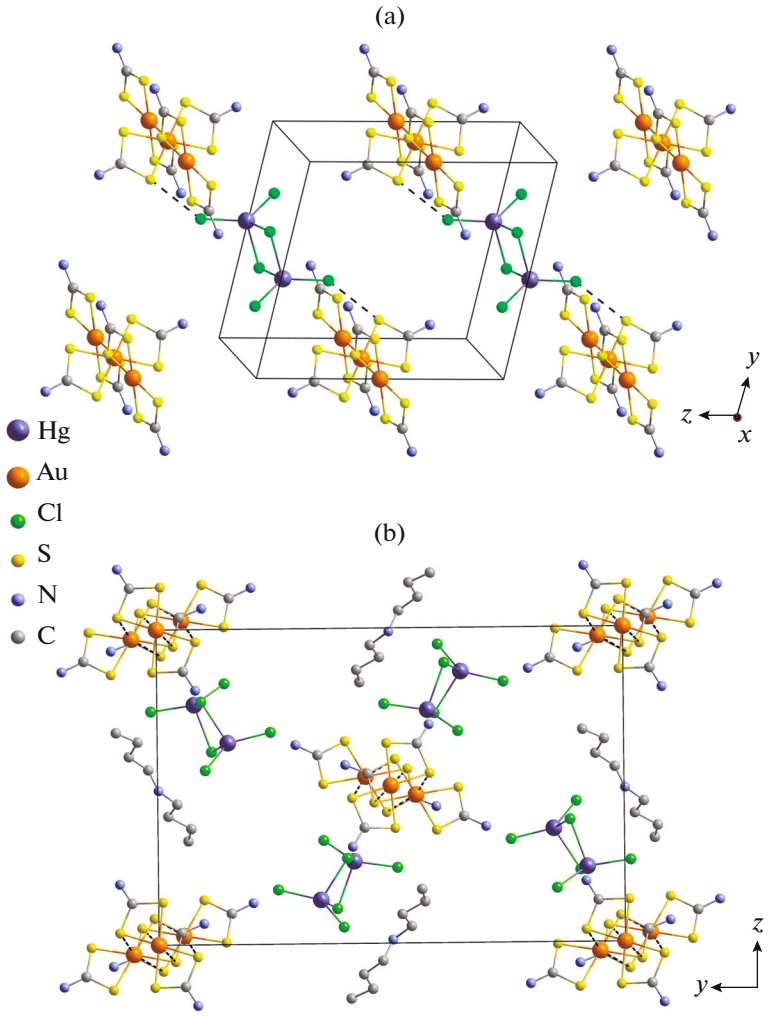

Fig. 1. Packing of structural units in the crystals of compounds (a) **I** and (b) **II**. Alkyl substituents of the BuDtc ligands are omitted.

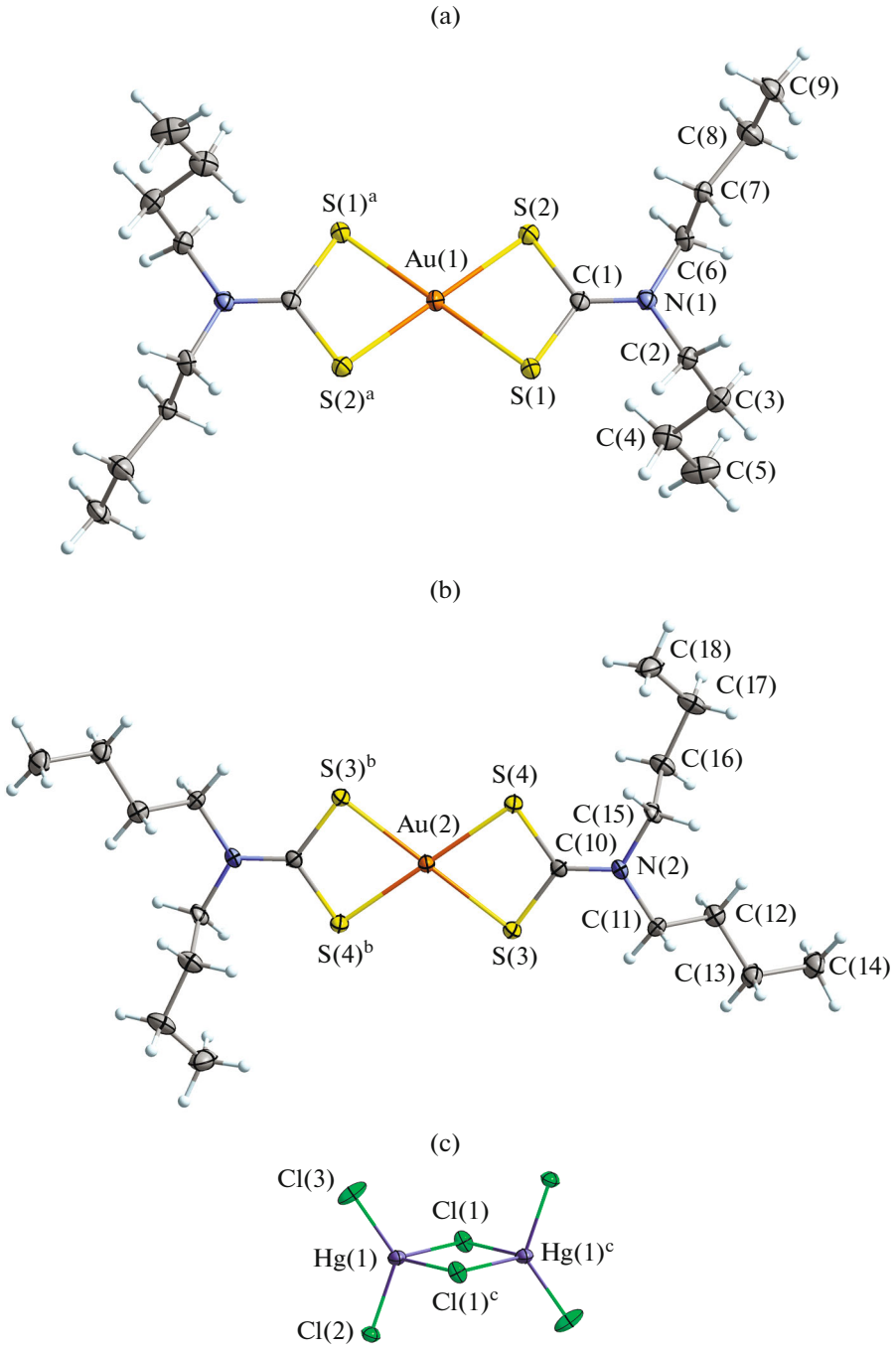

Fig. 2. Structures of two crystallographically independent gold(III) cations (a) A and (b) B and (c) binuclear anion $[Hg_2Cl_6]^{2-}$ in compound **I**. Ellipsoids are drawn at the 50% probability level.

complexes, the reliable differences in their geometric characteristics (bond lengths, interatomic distances, bond angles and torsion angles) allow one to classify the discussed complex gold(III) cations as conformational isomers.

The structures of both compounds include the binuclear anions $[Hg_2Cl_6]^{2-}$ (Hg(1)···Hg(1)^c 3.7403(2) Å (**I**) and Hg(1)···Hg(2) 3.7824(3) Å (**II**)), whose the mercury atoms, combined by two bridging chlorine atoms, form a distorted tetrahedral environment $[HgCl_4]$ (sp^3 hybrid state). A substantial distinction is that the structure of compound **I** includes the centrosymmetric complex anions (Fig. 2c), whereas a less typical, noncentrosymmetric version of their construction occurs in compound **II** (Fig. 3d). The central part of the complex anions is the four-membered metallocy-

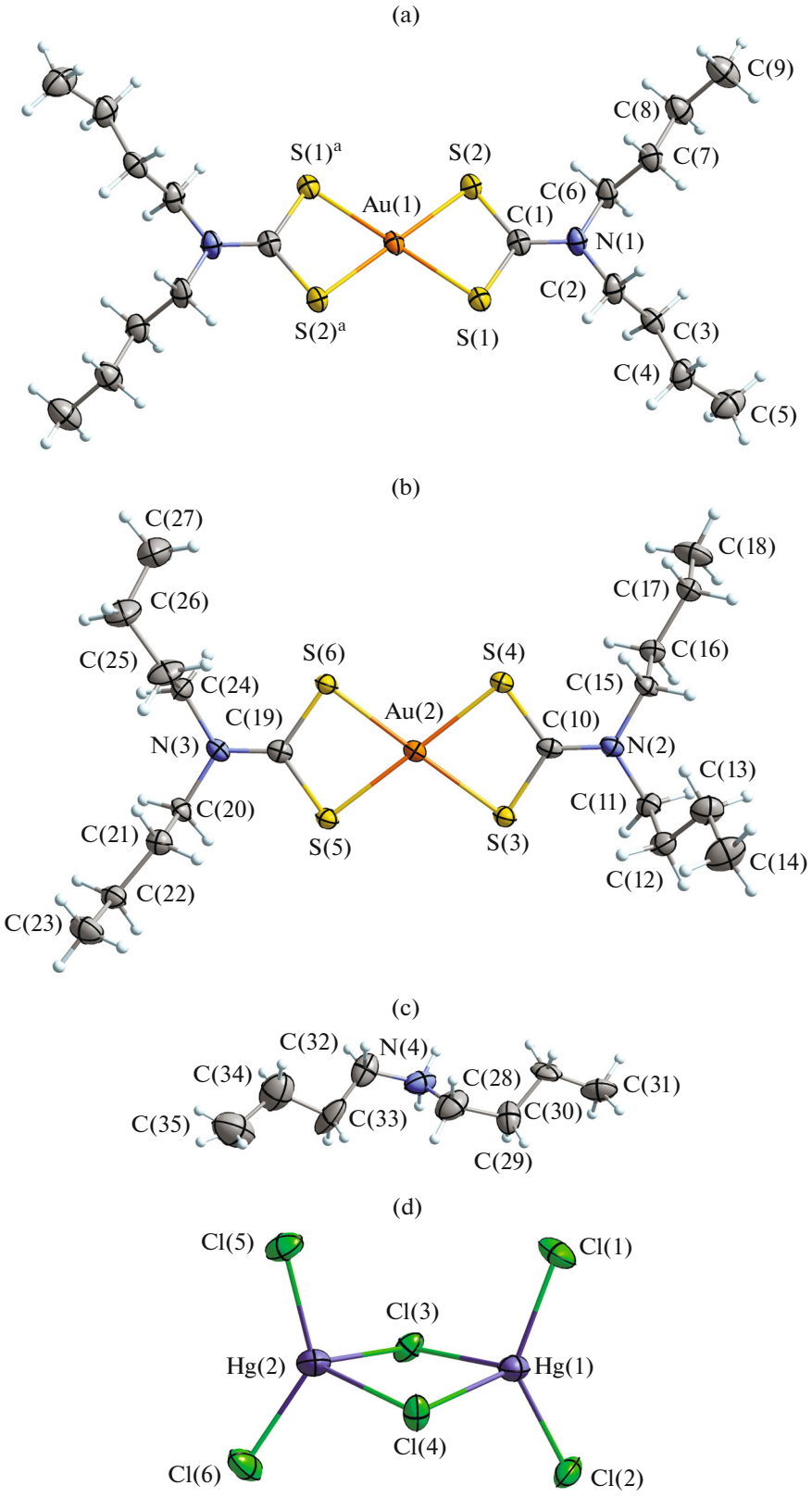

Fig. 3. Structures of two isomeric Au(III) cations (a) A and (b) B, (c) cation $[NH_2(C_4H_9)_2]^+$, and (d) binuclear anion $[Hg_2Cl_6]^{2-}$ in compound **II**. Ellipsoids are drawn at the 50% probability level.

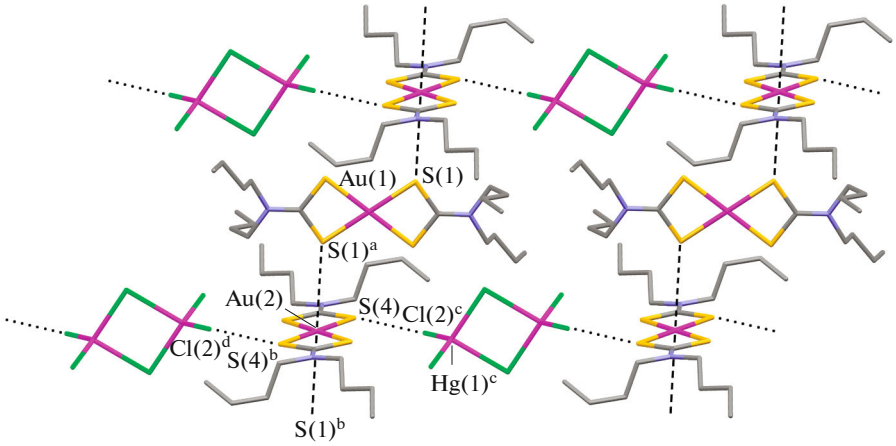

Fig. 4. Construction of the supramolecular 2D pseudo-polymeric layer in compound **I**: secondary bonds in the cation-anionic chains (arranged horizontally) S···Cl are shown by dotted lines, and short contacts Au···S between the nonequivalent gold(III) cations are shown by dashed lines. Symmetry transforms: [a] $-x, -y, 1-z$; [b] $1-x, -y, 1-z$; [c] $1-x, 1-y, 1-z$; [d] $1-x, 1-y, -z$.

cle $[Hg_2Cl_2]$, which is characterized (in complex **I**) by a planar configuration (torsion angles HgClClHg and ClHgHgCl are 180°). The discussed cycle in compound **II** adopts the butterfly conformation, which can be represented as a bend of the central $[Hg_2Cl_2]$ moiety along the Hg–Hg or Cl–Cl axis (the corresponding torsion angles ClHgHgCl and HgClClHg are 161.19° and 161.75°, respectively). The bonds of the central mercury atom with the terminal chlorine atoms are stronger (2.3660, 2.3984/2.3660–2.3879 Å) than those with the bridging atoms (2.5653, 2.6982/2.6200–2.6963 Å) (Table 2). The ClHgCl bond angles (89.47°–127.46°/87.26°–133.72°) (Table 2) deviate from the purely tetrahedral value, which is generally characteristic of halomercurate(II) ions [20–22]. In compounds **I** and **II**, the geometry of the mercury(II) polyhedra can quantitatively be characterized by the parameter $\tau_4 = [360° - (\alpha + \beta)]/141°$, where α and β are two largest LML angles in the complexes with the fourfold coordination of the central metal atom [23]. The limiting values of τ_4 equal to 1 ($\alpha = \beta = 109.5°$) or 0 ($\alpha = \beta = 180°$) indicate that a perfect tetrahedral or a regular square-planar geometry occurs for the coordination spheres of the $[ML_4]$ type. The data in Table 2 made it possible to calculate the τ_4 parameters for complexes **I** (0.831) and **II** (0.800 [Hg(1)] and 0.832 [Hg(2)]). Therefore, the $[HgCl_4]$ polyhedra are characterized by a distorted tetrahedral structure with the predominant (80.0–83.2%) contribution of the tetrahedral state to their geometry.

The supramolecular structures of the studied compounds are significantly different, although in both cases their formation is due to relatively weak secondary Au···S and S···Cl interactions of the nonvalent type between the isomeric Au(III) cations and Hg(II) anions. (The concept of secondary bonds was proposed earlier [24].) Let us consider the structural self-organization of complexes **I** and **II** in more detail.

In compound **I**, the isomeric Au(III) cations perform various structural functions. Each cation B forms secondary S···Cl bonds [25] with two nearest binuclear mercury(II) anions and *vice versa*. The construction of the discussed S(4)···Cl(2) bonds (3.3070(13) Å; cf. datum for the sum of the van der Waals radii of the sulfur and chlorine atoms, 3.55 Å [18, 19]) is carried out by two diagonally oriented S(4) and S(4)[b] atoms of cation B and two terminal Cl(2) and Cl(2)[c] atoms of the $[Hg_2Cl6]^{2-}$ anion, which results in the formation of cation-anionic supramolecular chains of the $(\cdots B\cdots[Hg_2Cl_6]^{2-}\cdots)_n$ type with the interatomic distance Au(2)–Hg(1) of 5.8010(2) Å (Fig. 4). In turn, cations A localized between the discussed chains interact with cations B *via* the diagonal S(1) and S(1)[a] sulfur atoms, thus participating (due to relatively weak secondary interactions Au(2)···S(1)[a] (3.6608 Å)) in the pairwise combination of supramolecular chains into a 2D pseudo-polymeric layer (Fig. 4).

The subsystem of alternating isomeric Au(III) cations linked by the above secondary interactions Au(2)···S(1) can also be considered as a set of linear supramolecular chains $(\cdots A\cdots B\cdots)_n$ oriented along the crystallographic axis *x* (interatomic distance Au(1)–Au(2) is 5.3200(2) Å). The mutual spatial orientation of neighboring cations in the chain (Fig. 5) is characterized by an angle of 80.51° between the planes in which the $[AuS_4]$ chromophores lie. The Au(2) atom in cation B builds up its nearest environment to a distorted elongated $[AuS_{4+2}]$octahedron due to the secondary interactions. The vertex sulfur atoms in the discussed octahedron are shifted from the ideal positions, since the S(1)[a]···Au(2)···S(1)[b] axis forms with the equatorial plane an angle of 70.47°, which deviates substantially from 90°. The equatorial plane of the

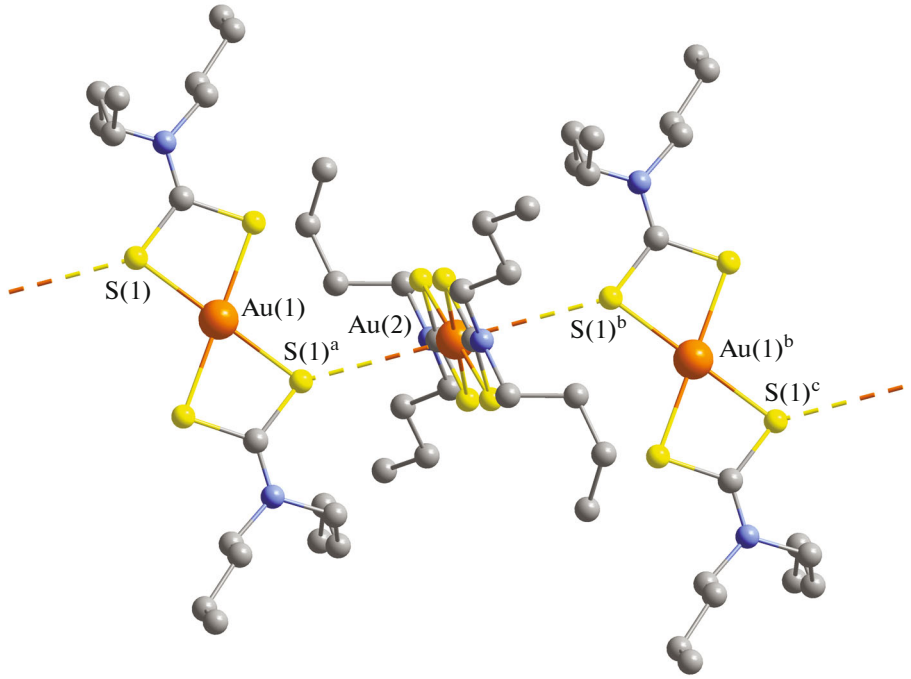

Fig. 5. Mutual spatial orientation of nonequivalent gold(III) cations A and B in the structure of compound **I**. Secondary interactions Au(2)···S(1)[a] are shown by double-dashed lines.

octahedron is determined by the sulfur atoms S(3), S(4), S(3)[b], and S(4)[b] forming a rectangle with the sides S(3)···S(4) (2.867 Å) and S(3)···S(4)[b] (3.695 Å), whose internal angles are close to the right angle: S(4)S(3)S(4)[b] is 89.71° and S(3)S(4)S(3)[b] is 90.29°.

Compound **II** contains the following structural units: three isomeric Au(III) cations (centrosymmetric cation A and two noncentrosymmetric cations B), two noncentrosymmetric $[Hg_2Cl_6]^{2-}$ anions, and the dibutylammonium cation $[(C_4H_9)_2NH_2]^+$ randomly distributed between two structural positions (with equal populations) (Fig. 3). All complex ions listed above are involved in the supramolecular organization of compound **II**. The isomeric gold(III) cations bound by pairs of substantially nonequivalent secondary bonds Au(2)···S(1) (3.2948 Å) and Au(1)···S(6) (3.5698 Å) (the sum of the van der Waals radii of the gold and sulfur atoms is 3.46 Å [18, 19]) form linear supramolecular triads $[B···A···B]^{3+}$: the interatomic distance Au(1)–Au(2) is 4.0649(3) Å and the Au(2)Au(1)Au(2) angle is 180°. Noncentrosymmetric cations B are antiparallel, whereas the planes of the $[AuS_4]$ chromophores of neighboring cations A and B form an angle of 16.95° (Fig. 6a). In turn, the cationic triads build zigzag pseudo-polymeric chains $(···[B···A···B]···)_n$ oriented along the crystallographic axis *x* due to the relatively weak symmetric secondary interactions Au(2)···S(5)[a] and Au(2)[a]···S(5) (3.8655 Å) (Fig. 6a): the Au(2)–Au(2) distance between the triads is 5.0552(3) Å and the Au(1)Au(2)Au(2) angle is 124.61°.

However, the main contribution to the binding of the discussed cationic triads [B···A···B] is made by secondary interactions with the noncentrosymmetric anions $[Hg_2Cl_6]^{2-}$ (Fig. 7). In this case, the terminal chlorine atoms Cl(1) and Cl(2) of the binuclear mercury(II) anions localized between the cationic pseudo-polymeric chains and the sulfur atoms S(3) and S(4) of one of the ligand in each of two antiparallel cations B (belonging to the neighboring cationic triads) form two pairs of nonequivalent secondary bonds S(3)···Cl(1) (3.4014(16) Å) and S(4)···Cl(2) (3.4940(13) Å). In addition, another pair of chlorine atoms (terminal Cl(6) and bridging Cl(3)) is involved in the formation of hydrogen bonds with the dibutylammonium cation (which in each structural position is equiprobably presented by one of two opposite orientations): N(4)–H(41*B*)···Cl(3) (3.412(7) Å) and N(4)–H(42*B*)···Cl(6)[d] (3.481(8) Å) (Fig. 7, Table 3). As a result, three-membered structural fragments $\{[Hg_2Cl_6]^{2-}···[(C_4H_9)_2NH_2]^+···[Hg_2Cl_6]^{2-}\}$ are formed (Fig. 6b), which link the nearest cationic pseudo-polymeric chains at the edges of the cationic triads of the cationic triads [B···A···B]. Thus, the overall manifestation of all discussed interactions leads to the total binding of the ionic structural units of compound **II** into a 3D supramolecular framework (Fig. 7).

The most significant secondary bonds Au···S are formed in the cationic triads due to which the gold

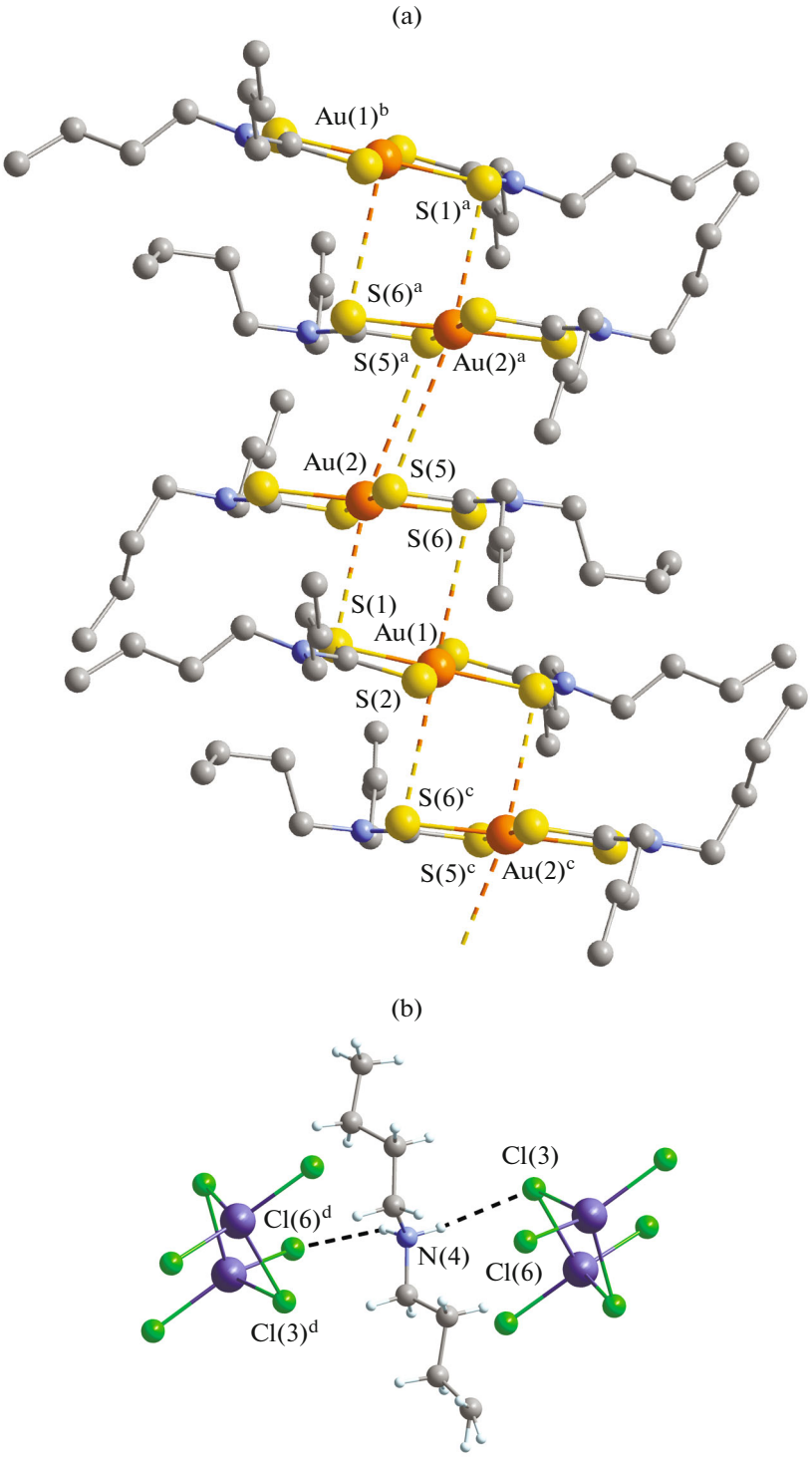

Fig. 6. (a) Fragment of the supramolecular cationic chain $(\cdots[B\cdots A\cdots B]\cdots)_n$ in compound **II** (secondary bonds Au···S are shown by double-dashed lines) and (b) structure of the three-membered fragment $\{[Hg_2Cl_6]^{2-}\cdots[NH_2(C_4H_9)_2]^{+}\cdots[Hg_2Cl_6]^{2-}\}$ (hydrogen bonds are shown by dashed lines). Symmetry transforms: [a] $1-x, 1-y, 1-z$; [b] $1+x, y, z$; [c] $-x, 1-y, 1-z$; [d] $1-x, 1-y, -z$.

atoms build up their polygon to a distorted tetragonal pyramid $[Au(2)S_{4+1}]$ and distorted octahedron $[Au(1)S_{4+2}]$. In an elongated pyramid, the vertex S(1) atom is shifted from an ideal position, because the S(1)···Au(2)–S(4) angle (82.29°) deviates noticeably from 90°. In an elongated octahedron, the effect of displacement of axial atoms is less pronounced: the S(6)···Au(1)···S(6)^c axis forms an angle of 86.99° with

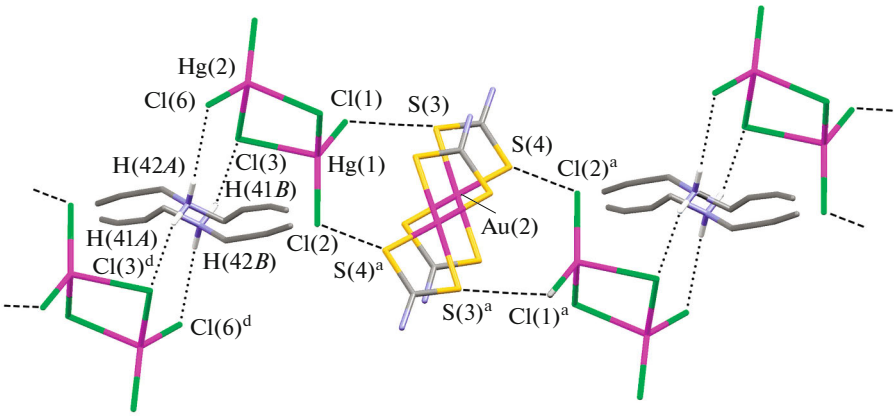

Fig. 7. Fragment of the supramolecular structure of compound **II**: secondary bonds S···Cl are shown by dashed lines, and hydrogen bonds between the $[Hg_2Cl_6]^{2-}$ anions and dibutylammonium cations are shown by dotted lines. Dibutylammonium cations are randomly distributed between two positions with equal populations. Symmetry transforms: [a] $1-x, 1-y, 1-z$; [d] $1-x, 1-y, -z$.

the equatorial plane. The sulfur atoms in the basal plane of the discussed pyramid and in the equatorial plane of the octahedron form almost regular rectangles, whose short and long sides lie in relatively narrow ranges of 2.846–2.864 and 3.689–3.734 Å, respectively, and the internal SSS angles are close to the right angle: 89.38°–90.63°.

The ^{13}C CP-MAS NMR spectrum of the crystalline material obtained for XRD expectedly exhibits the resonance signals of the >NC(S)S–, >N–$^{\alpha}CH_2$–, –$^{\beta}CH_2$–, –$^{\gamma}CH_2$–, and –CH_3 groups (Fig. 8). The most resolved and structurally informative range of the dithiocarbamate groups is represented by four ^{13}C signals (with the ratio of integral intensities close to 1 : 2 : 1 : 1), whose chemical shift values (196.0, 195.7, 195.4, and 195.1 ppm) indicate that the BuDtc ligands are localized in the inner sphere of gold(III) [26–28]. Complexes **I** and **II** contain two and three nonequivalent BuDtc ligands, respectively, which is completely consistent with the observed number and ratio of integral intensities in the discussed group of ^{13}C resonance signals, being the result of the superposition of the doublet (1 : 1) and triplet (1 : 1 : 1). Thus, the reaction presented in the section Synthesis of complexes **I** and **II** determines the formed substances and also correctly specifies their quantitative ratio.

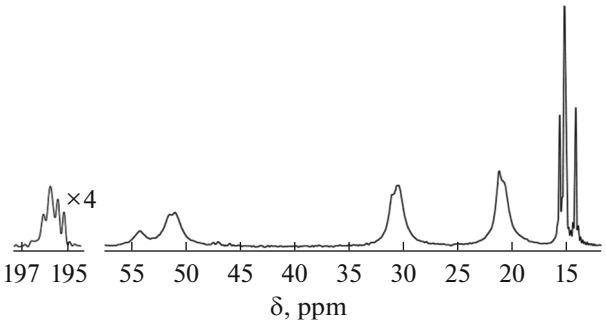

Fig. 8. ^{13}C CP-MAS NMR spectrum of the crystals obtained for XRD (rotation frequency of the sample 3.2 kHz, acquisition number 6900).

The thermal behavior of the complexes was studied by STA using parallel detection of TG and DSC curves. Crystalline complexes **I**/**II** were found to be thermally stable below 176/165°C. Then the TG curve records the multistage process of thermal destruction of the obtained compounds (Figs. 9a, curve *1*; 9b, curve *1*). The differentiation of the first steeply descending step (176–301/165–308°C) related to the main mass loss (67.68/71.01%) makes it possible to reveal two inflection points (at 233/221 and 272/281°C), which divide the step into three segments. These reveal a complicated character of thermolysis, comprising the reduction of Au(III) to the elemental state, liberation of $HgCl_2$, and its partial transformation into HgS. The characteristic step of mass loss is observed in the range of 301–365/308–386°C, which is usually typical of the Au(III)–Hg(II) dithiocarbamato-chlorido complexes [10] and is related to thermal dissociation of the formed HgS [29, 30]. The experimental mass loss at this step (6.32/7.16%) indicates that at least 24.8/24.4% of the total amount of mercury in the sample is transformed into HgS. Thus, the remaining part of mercury(II) is liberated in the form of $HgCl_2$ (calcd. 22.37/25.86%), whose sublimation precedes the thermal decomposition of HgS [10] or overlaps it [30]. In our case, the region with the mass loss 9.67/8.31% in the range of 272–301/281–308°C (after the second inflection point), whose boundaries are close to m.p. and b.p. values of $HgCl_2$, precedes the discussed step of mercury(II) sulfide decomposition [31]. However, the experimental mass loss is sig-

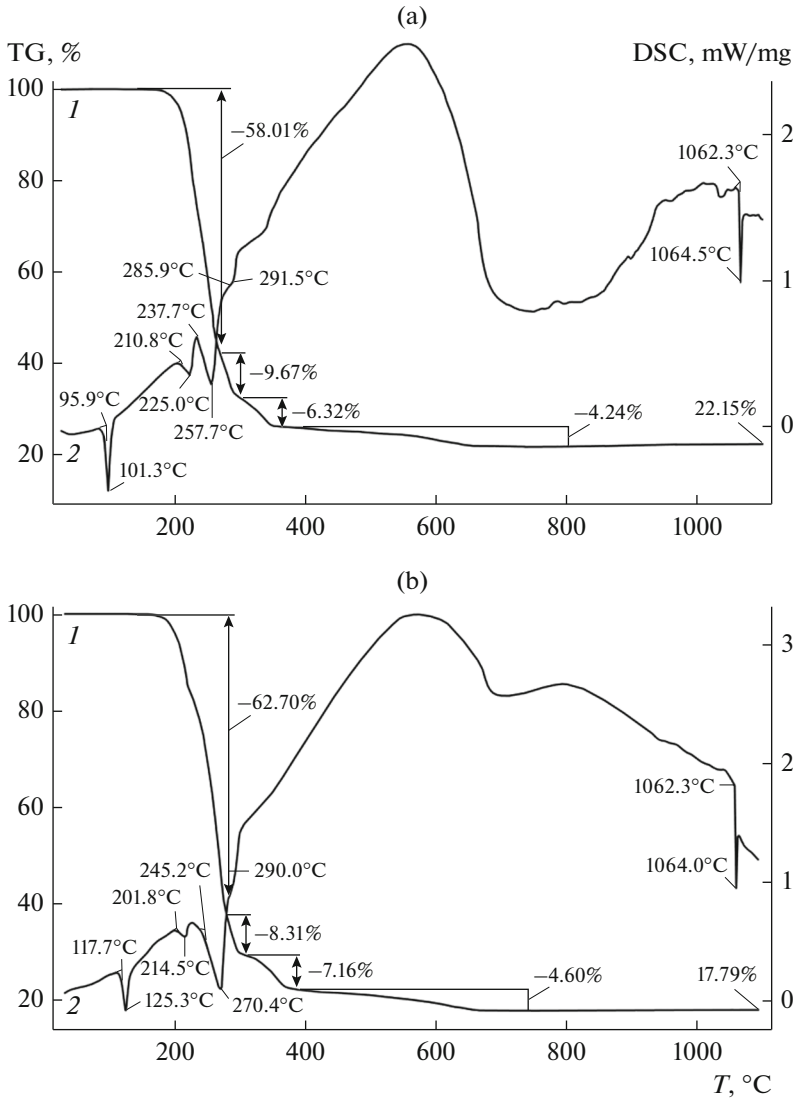

Fig. 9. (*1*) TG and (*2*) DSC curves for complexes (a) **I** and (b) **II**.

nificantly lower than the calculated value, indicating the sublimation of the major amount of $HgCl_2$ still before the m.p. is riched. (The latter is consistent with published results [10].) The observed mass loss in the first step of the TG curve before the second inflection point is 58.01/62.70%, which, on the one hand, considerably exceeds the theoretically expected value (45.49/43.77%), and, on the other hand, completely overlaps the missing mass loss of $HgCl_2$. The flat region of the TG curve (365–801/385–743°C) is associated with the final desorption (4.24/4.60%) of the thermolysis products. The residual mass at 1100°C (22.15/17.79%) somewhat deviates from the value calculated for reduced gold (calcd. 21.58/18.61%), fine balls of which are observed when the crucible is opened.

The DSC curve for complexes **I** and **II** has several thermal effects (Figs. 9a, curve *2*; 9b, curve *2*). The first endotherm with an extremum at 101.3/125.3°C, detected in the range of thermal stability of the complexes, reflects their melting (extrapolated m.p. = 95.9/117.7°C). The melting of the samples during the independent determination in a glass capillary was found in the range of 94–96/118–120°C. Three subsequent endotherms with extrema at 225.0/214.5, 257.7/270.4, and 291.5/290.0°C (the latter was revealed by the differentiation of the DSC curve) are projected onto the first, second, and third segments, respectively, of the main mass loss step. For each of compounds **I** and **II**, the DSC curve shows the high-temperature endotherm of melting of reduced gold: extrapolated m.p. = 1062.3°C.

Thus, new pseudo-polymeric crystalline gold(III)–mercury(II) complexes $([Au\{S_2CN(C_4H_9)_2\}_2]_2[Hg_2Cl_6])_n$ and $([(C_4H_9)_2NH_2]_{0.5}[Au\{S_2CN(C_4H_9)_2\}_2]_{1.5}[Hg_2Cl_6])_n$ were preparatively iso-

lated and characterized by the XRD and ^{13}C CP-MAS NMR techniques. The structural units of the complexes participate in the construction of the complicatedly organized 1D, 2D, and 3D supramolecular aggregates. The secondary interactions Au···S and S···Cl, as well as hydrogen bonds N–H···Cl, play the determining role in their supramolecular self-assembly. The quantitative regeneration of bound gold under relatively mild conditions was found by the study of the thermal behavior of the synthesized substances.

ACKNOWLEDGMENTS

The authors are grateful to Prof. O.N. Antzutkin (Luleå University of Technology, Luleå, Sweden) for the kindly presented opportunity of ^{13}C CP-MAS NMR spectra recording.

CONFLICT OF INTEREST

The authors declare that they have no conflicts of interest.

REFERENCES

1. Priola, E., Bonometti, E., Brunella, V., et al., *Polyhedron*, 2016, vol. 104, p. 25.
2. Amani, V., Alizadeh, R., Alavije, H.S., Heydari, S.F., and Abafat, M., *J. Mol. Struct.*, 2017, vol. 1142, p. 92.
3. Rajarajan, M., *Novus Int. J. Chem.*, 2013, vol. 2, no. 1, p. 1.
4. Onwudiwe, D.C. and Ajibade, P.A., *Mater. Lett.*, 2011, vol. 65, nos. 21–22, p. 3258.
5. Dar, S.H., Thirumaran, S., and Selvanayagam, S., *Polyhedron*, 2015, vol. 96, p. 16.
6. Manohar, A., Ramalingam, K., and Karpagavel, K., *Int. J. ChemTech Res.*, 2014, vol. 6, no. 5, p. 2620.
7. Prasad, R., Yadav, R., Trivedi, M., et al., *J. Mol. Struct.*, 2016, vol. 1103, p. 265.
8. Loseva, O.V., Rodina, T.A., Smolentsev, A.I., and Ivanov, A.V., *Russ. J. Coord. Chem.*, 2016, vol. 42, no. 11, p. 719. https://doi.org/10.1134/S1070328416110063
9. Loseva, O.V., Rodina, T.A., and Ivanov, A.V., *Russ. J. Gen. Chem.*, 2019, vol. 89, no. 11, p. 2273. https://doi.org/10.1134/S1070363219110185
10. Loseva, O.V., Rodina, T.A., Smolentsev, A.I., and Ivanov, A.V., *Polyhedron*, 2017, vol. 134, p. 238.
11. Loseva, O.V., Rodina, T.A., Antzutkin, O.N., and Ivanov, A.V., *Russ. J. Gen. Chem.*, 2018, vol. 88, no. 12, p. 2540. https://doi.org/10.1134/S1070363218120149
12. Ivanov, A.V., Sergienko, V.I., Gerasimenko, A.V., et al., *Russ. J. Coord. Chem.*, 2010, vol. 36, no. 5, p. 353. https://doi.org/10.1134/S1070328410050064
13. Rodina, T.A., Loseva, O.V., Smolentsev, A.I., and Ivanov, A.V., *J. Struct. Chem.*, 2016, vol. 57, no. 1, p. 146. https://doi.org/10.1134/S0022476616010182
14. Byr'ko, V.M., *Ditiokarbamaty* (Dithiocarbamates), Moscow: Nauka, 1984.
15. Cox, M.J. and Tiekink, E.R.T., *Z. Kristallogr.*, 1999, vol. 214, no. 9, p. 571.
16. *APEX2 (version 1.08), SAINT (version 7.03), SADABS (version 2.11), SHELXTL (version 6.12)*, Madison: Bruker AXS Inc., 2004.
17. Pines, A., Gibby, M.G., and Waugh, J.S., *J. Chem. Phys.*, 1972, vol. 56, no. 4, p. 1776.
18. Pauling, L., *The Nature of the Chemical Bond and the Structure of Molecules and Crystals*, London: Cornell Univ., 1960.
19. Bondi, A., *J. Phys. Chem.*, 1964, vol. 68, no. 3, p. 441.
20. Exarchos, G., Robinson, S.D., and Steed, J.W., *Polyhedron*, 2001, vol. 20, nos. 24–25, p. 2951.
21. Elwej, R., Hannachi, N., Chaabane, I., et al., *Inorg. Chim. Acta*, 2013, vol. 406, p. 10.
22. Castiñeiras, A., García-Santos, I., and Saa, M., *Acta Crystallogr., Sect, C: Struct. Chem.*, 2019, vol. 75, p. 891.
23. Yang, L., Powel, D.R., and Houser, R.P., *Dalton Trans.*, 2007, no. 9, p. 955.
24. Alcock, N.W., *Adv. Inorg. Chem. Radiochem.*, 1972, vol. 15, no. 1, p. 1.
25. Haiduc, I. and Edelmann, F.T., *Supramolecular Organometallic Chemistry*, New York: Wiley-VCH, 1999.
26. Rodina, T.A., Ivanov, A.V., Gerasimenko, A.V., et al., *Polyhedron*, 2012, vol. 40, no. 1, p. 53.
27. Rodina, T.A., Filippova, T.S., Ivanov, A.V., et al., *Russ. J. Inorg. Chem.*, 2012, vol. 57, no. 11, p. 1490. https://doi.org/10.1134/S0036023612110113
28. Korneeva, E.V., Smolentsev, A.I., Antzutkin, O.N., and Ivanov, A.V., *Russ. Chem. Bull., Int. Ed.*, 2019, vol. 68, no. 1, p. 40. https://doi.org/10.1007/s11172-019-2413-7
29. Leckey, J.H. and Nulf, L.E., *Thermal Decomposition of Mercuric Sulfide*. 1994. https://doi.org/10.2172/41313
30. Angeloski, A., Rawal, A., Bhadbhade, M., et al., *Cryst. Growth Des.*, 2019, vol. 19, p. 1125.
31. Lidin, R.A., Andreeva, L.L., and Molochko, V.A. *Spravochnik po neorganicheskoi khimii* (Reference Book in Inorganic Chemistry), Moscow: Khimiya, 1987.